New Journal of Physics
The open-access journal for physics

A two-dimensional cold atmospheric plasma jet array for uniform treatment of large-area surfaces for plasma medicine

QY Nie[1,2,3], Z Cao[1,3], C S Ren[2], D Z Wang[2] and M G Kong[1,4]

[1] Department of Electronic and Electrical Engineering, Loughborough University, Leicestershire LE11 3TU, UK
[2] School of Physics and Optoelectronic Technol, Dalian University of Technology, People's Republic of China
E-mail: m.g.kong@lboro.ac.uk

New Journal of Physics **11** (2009) 115015 (14pp)
Received 3 August 2009
Published 26 November 2009
Online at http://www.njp.org/
doi:10.1088/1367-2630/11/11/115015

Abstract. For plasma treatment of inanimate surfaces and living tissues in medicine, it is important to control plasma–sample interactions and to mitigate non-uniform treatments of usually uneven sample surfaces so that effectiveness of application can be reproduced for different biological samples, relatively independently of their varying surface topologies and material characters. This paper reports a scalable two-dimensional (2D) array of seven cold atmospheric plasma (CAP) jets intended to achieve these two important requirements as well as to address the unique challenge of jet–jet interactions. While the CAP jet array can be configured to interact with a biological sample in either a direct mode (used with an *in situ* sample) or a remote mode (used as an afterglow), this study focuses on the direct mode. Using a downstream planar electrode as a sample model, the spatial distribution of reactive species and electrons delivered by individual jets of the 2D CAP jet array attains excellent uniformity. Specifically, the spatial variation over 100 μs is 5.6 and 7.9%, respectively, for wavelength-integrated optical emission intensity, and for atomic oxygen emission intensity at 845 nm when the oxygen admixture is 0.5% of the helium carrier gas. It is also shown that the highest emission intensity at 845 nm occurs at $O_2/He = 0.5\%$ under the best jet–jet uniformity conditions for $O_2/He = 0.3$–0.7%. These results indicate the potential of 2D CAP jet arrays for

[3] These two authors made equal contributions.
[4] Author to whom correspondence should be addressed.

uniform treatment and for effective control of jet–jet interactions. Furthermore, spatial uniformity is accompanied by rich dynamics of jet–jet interactions and jet–sample interactions. Of the honeycomb-arranged seven CAP jets, the central jet is strongest in the negative half cycle, whereas the six surrounding jets (of uniform strength) are strongest in the positive half cycle. These dynamic features offer possible insights with which to better control jet–jet interactions and plasma–surface interactions in future.

Contents

1. Introduction

One key enabler for the rapid expansion of plasma medicine is the advance of cold atmospheric plasmas (CAPs) that can be placed in direct contact with plant, animal and human tissues without the need for a vacuum chamber [1]–[3]. As a rich source of reactive plasma species, radicals and UV photons [4]–[6], these open-air plasmas offer a chamber-free route to surface modifications to both inanimate objects and living tissues, often with little damage from energetic electrons and ions. Their distinctive biological effects have the potential to be developed into new plasma-enabled healthcare solutions with applications in hospital disinfection [7]–[10] and food decontamination [11]–[14], skin disease and cancer therapies [15]–[18], and wound care and wound healing [1]–[3]. To achieve widespread use in medicine, however, the typically small CAP sources must be scaled up and be capable of treating uneven and sometimes wet surfaces, for example open wounds and complex surgical instruments. These areas of plasma medicine are not best addressed by individual CAP jets with a diameter of a few millimetres or less [19]–[22], as their small size restricts their use in localized applications such as precision cell manipulation [23] and dentistry [24]–[26]. Instead, large CAP sources with a length of many tens of centimetres are needed. This is actually a very difficult challenge, particularly with the stringent medical demand for processing reproducibility in context of great variation in sample materials and their surface topology (i.e. uneven human skins and wounds). To this end, two basic requirements must be considered in the current development of CAP sources, namely effective control of plasma–surface interactions and improved uniformity of CAP treatments of uneven surfaces [27]. This paper reports a first attempt at meeting such requirements using a two-dimensional (2D) array of CAP jets.

The current options for large-scale CAP sources are rather limited. They include floating-electrode dielectric-barrier discharges (FE-DBD) [1, 16], afterglow extended from discharges between parallel porous electrodes [3, 28, 29], or afterglow of microwave plasmas [30]–[32]. Often with flat surfaces of contaminated samples, these large CAP sources have been used to encouraging effect [1, 3, 16, 29, 32]. However, plasma–surface interaction and treatment

uniformity on a large scale are yet to be addressed in the published literature, and furthermore the reported data are yet to be evaluated for uneven surfaces. These indicate an early developmental stage for large-scale CAP sources for plasma medicine, and highlight the need to develop current and future CAPs specifically for the needs of their intended medical applications. The challenge is, however, complex, involving several intertwined and sometimes conflicting considerations. Plasma–surface interactions may be minimized by placing a sample towards the end of an afterglow, possibly at the expense of the application efficacy, whereas the need to maximize CAP effects would favour direct sample contact with the light-emitting part of the plasma, making plasma stability more susceptible to surface variation in the sample. Also, current uncertainty over the identity of responsible plasma species in plasma medicine makes it difficult to determine the location of the sample with respect to the plasma; the light-emitting part of an atmospheric plasma is likely to contain abundant charged particles, whereas its afterglow may contain mainly neutral species. An empirical strategy may lead to a solution for one application. However, with the need to repeat for different applications this is an expensive approach, and it may result in a compromise rather than an optimization of what the CAP technology can offer.

As an alternative large CAP source to FE-DBD and atmospheric afterglows, this work investigates a class of 2D CAP jet arrays that can be up-scaled and has an inbuilt mechanism to control the plasma–sample interactions. A unique challenge of CAP jet arrays is that individual plasmas in an array tend to interact very strongly and this can lead to quenching of some individual plasmas. To this end, we focus in this study on how the jet–jet interaction may affect the spatial uniformity of reactive plasma species delivered by individual plasma jets to the surface of a downstream flat sample. The issue of uneven sample surfaces is important, but could, in principle, be addressed effectively using individual ballasts [27]. This will be reported on in a future note. In this work, we consider the mode of direct plasma–sample interaction in which the light-emitting part of the CAP jet array contacts the downstream sample directly, and an electric current runs through the sample. This mode of plasma–sample interactions is similar to that in FE-DBD, with the sample being treated with both neutral and charged species. If future mechanism studies suggest that neutral species provided by an atmospheric afterglow are the most essential for plasma medicine and their concentrations are adequate, the CAP jet arrays can be readily configured in an afterglow configuration with the sample simply placed outside the light-emitting part of the plasmas. In other words, the CAP jet arrays could be used to acquire the character of either FE-DBD or afterglows, depending on the application required.

As an indirect measure of reactive plasma species, we employ wavelength-filtered optical emission at the jet contact points on the surface of a downstream planar sample. Spatial distribution of the latter is then used to indicate the uniformity of plasma-delivered reactive species and hence the uniformity of plasma treatment. Specifically, we consider the helium emission line at 706 nm as an indicator of energetic electrons and the two atomic oxygen lines at 777 and 845 nm as indicators of reactive oxygen species. Together, they are representative of key plasma agents. As a platform source with scalability, and given an inherent jet–jet interaction in CAP jet arrays, we consider a seven-CAP-jet array arranged two-dimensionally in a honeycomb configuration with a flat downstream electrode as the planar sample. Following a discussion of the jet array arrangement, its electrical characterization and nanosecond-resolved imaging are used to establish its difference from a typical single-jet device, and the dynamic evolution of all its seven jets. These provide a direct description of jet–jet interaction and the plasma stability of the jet array, both being important factors in achieving uniform treatment and, ultimately,

processing reproducibility. Fast imaging with both the wavelength integrated and the wavelength filtered is then used to obtain the spatial distribution of the optical emission intensities of individual jets and to evaluate their spatial uniformity. Finally, the treatment uniformity obtained from wavelength-resolved fast imaging is examined for its reliance on different oxygen–helium mixtures, and on variation of the applied voltage. This is important for establishing whether the best uniformity and the most active reaction chemistry may be mutually exclusive.

2. Two-dimensional (2D) configuration of CAP jets

Two-dimensional arrays of spatially confined CAPs have been reported on, particularly those employed by the groups of Eden [33] and Tachibana [34]. However, CAP jets are spatially extended out of their electrode region towards a downstream processing space and the spatial separation of plasma generation from plasma processing has been known to be effective to mitigate plasma–surface interactions [35]. For large objects with uneven surfaces, spatially extended atmospheric plasma arrays (SEAPA) are highly desirable [36]. The air plasma flames proposed by Kuo *et al* around 1998 are the only reported 2D array of atmospheric plasmas that might be regarded as having some degree of spatial extension [37, 38]. However, this early system may have too large a distance between two adjacent plasma sources to be suitable as a large-scale plasma source, and its high gas temperature could limit its use for plasma medicine. Subsequent development of one-dimensionally arranged CAP jet arrays offers much greater relevance to plasma medicine [27, 39, 40]. In particular, individual ballast and well engineered power electronics have facilitated a very effective control of both jet–jet interactions and plasma–surface interactions [27]. Against a dielectric substrate sloped at 15 °C and placed downstream, these control techniques have allowed a 10-CAP-jet array to reduce the spatial variation of downstream reactive species to below 12% from 48% in the case of a single CAP jet scanning across the sloped substrate. A 10-CAP-jet array is also capable of firing all 10 jets simultaneously onto the heavily 3D structure of a surgical forceps, though its treatment uniformity has not been evaluated. Such performances against uneven surfaces and 3D structures suggest the capability of the 1D CAP jet array to effectively control the plasma–surface interactions in the direct plasma–sample interaction mode.

With the same power electronics and similar jet-housing structures, the 2D array of seven CAP jets considered in this study is shown schematically in figure 1, with a honeycomb configuration showing its structural details with both side and end views. The diameter of the entire array was 10 mm. The dielectric tube was made of quartz with an inner diameter of 1.4 mm and an outer diameter of 2.9 mm, and the centre-to-centre distance between two adjacent quartz tubes was 3.55 mm. The seven jets were therefore tightly packed to maximize surface coverage of a downstream object with strong jet–jet interactions. The jet density, measured as the ratio of the plasma jet diameter to the jet–jet distance [36], was about 0.4. Usually at such a high jet density, jet–jet interactions are so strong that they cause repelled or converged jet channels, thus defeating the purpose of forming an array. A great many range-finding studies were performed before arriving at the array of well collimated jets shown in figure 1. The seven bright spots at the end of each CAP jet were measured from wavelength-integrated optical emission in a 100 μs exposure time.

For the experiments reported here, the jet-housing structure in figure 1 supported seven identical channels, each of which consisted of a central capillary electrode enclosed tightly within a concentric quartz tube. The capillary doubled up as the gas inlet channel, and its tip

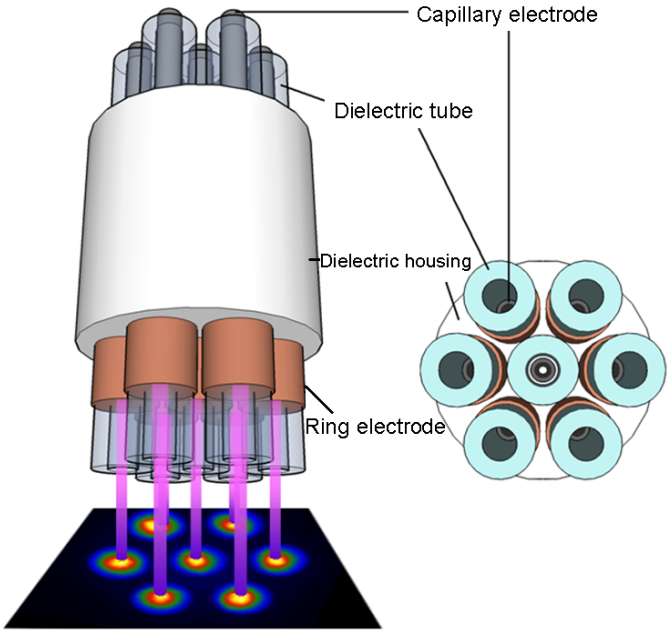

Figure 1. Schematic of the seven-jet array arranged in a honeycomb configuration with both side view (left) and end view (right). Each plasma jet delivers a jet-centric spread of reactive species on the downstream substrate. The seven circular images on the substrate are wavelength-integrated plasma emissions taken with a 100 μs exposure time.

was some distance in the axial direction away from a ring electrode wrapped near the end of the quartz tube. The ring electrode was grounded. The electric field set up between the two electrodes was largely axial and so each single jet was a linear-field jet device [41]. The capillary electrode is made of stainless steel with its inner and outer diameter being 0.838 and 1.27 mm, respectively. The annular gap between the quartz tube and the capillary was only 65 μm. An indium tin oxide (ITO) ground electrode was placed 13 mm downstream from the quartz tube nozzle, usually with its glass side facing the plasma jets. Helium (99.996%) was used as the carrier gas at 15 slm (standard litres per minute), and it was fed through each of the seven capillary electrodes at 2.14 slm. Oxygen was mixed into the helium flow with its admixture being 0.1–1%, but nominally at 0.5% or 75 sccm (standard cubic centimetres per minute) in a total helium rate of 15 slm.

The jet array was powered, via the capillary electrode of each of the seven jets, by an ac power supply at 10 kHz and with an amplitude adjustable up to 5 kV. The power electronics were considered and engineered carefully so that the power supply was well matched to the jet array even when the plasma–surface interaction was significant. The array-housing unit in figure 1 was found to have an in-built ballast function, though individual ballasts were not included in the external circuit. Voltage and current signals were measured with a Tektronix P6015AS 75 MHz high voltage probe and a Pearson 2877 1V/1A 200 MHz current probe, respectively, and recorded via a Tektronix DPO4104 oscilloscope (1 GHz bandwidth and 10 mega-bit sample record length). Plasma images were taken using an Andor DH720 camera with or without wavelength filters.

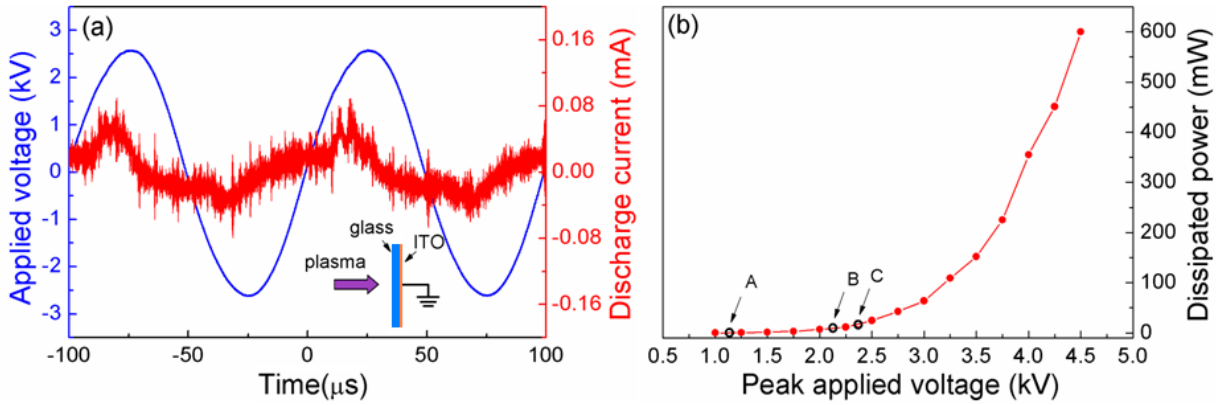

Figure 2. Electrical characteristics of the seven-jet CAP array addressing an ITO substrate with its glass facing the plasma jet: (a) time traces of the applied voltage and the total discharge current and (b) the voltage dependence of the total dissipated power. Points A, B and C in (b) indicate, respectively, the ignition point for the six outer jets (simultaneous ignition), the ignition point for the central jet, and the point where all seven jets reach the downstream ITO electrode. Helium flow is 15 slm and oxygen flow is 75 sccm.

3. Electrical characterization and plasma jet dynamics

For each jet, a small plasma was observed near the tip of the capillary electrode inside its quartz tube immediately after ignition. With increasing applied voltage, the plasma started to extend towards the ring electrode, and eventually emerged from the tube nozzle. Further increase to the applied voltage resulted in a plasma plume. The plasma plume extended with increasing voltage, before it reached the downstream ITO electrode. Figure 2(a) shows the temporal characters of the applied voltage and the total current of the jet array when $O_2/He = 0.5\%$ and the peak applied voltage was 2.6 kV with the downstream ITO electrode having its glass side facing the plasma. The discharge current is small with a peak voltage of around 0.07 mA, smaller than that of a single jet in a single-channel configuration (i.e. not in the array structure) and also smaller than that in the 1D 10-CAP-jet array [27]. The large variation on the current curve represents noise, because the low current value was close to the detection limit of the current probe. Simultaneous measurement of currents flowing in each of the seven channels was not possible, partly due to an undesirable effect on matching the plasma to the power supply by the introduction of seven current probes. However, our previous work on the 1D 10-CAP jet array showed a very good temporal synchronization between individual currents flowing in its 10 plasma channels [27]. We believe that a similar temporal synchronization between individual currents was present in the 2D CAP jet array of figure 1.

In the case of the jet array, it was observed that the six outer channels were broken down first but simultaneously, before plasma ignition was triggered in the central channel. Figure 2(b) shows the evolution of the dissipated power voltage dependence of the dissipated power, with points A, B and C representing the point of ignition of the six outer channels, the ignition point for the central channel, and the point of all seven jets reaching the downstream ITO electrode. Point C corresponds to a peak applied voltage of about $V_p = 2.4$ kV, and so the current trace at 2.6 kV in figure 2(a) was obtained shortly after the jets reached the substrate. Once the

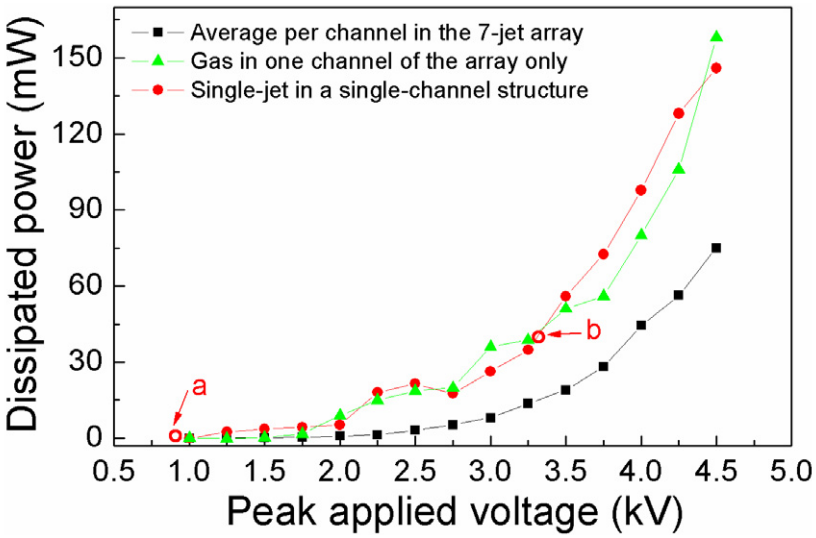

Figure 3. Voltage dependence of the dissipated power in one plasma channel in the case of the seven-jet array (black); gas flow and hence plasma formation in the central channel of the array structure (green, no plasma ignited in the six outer channels); and a single plasma in a single-jet electrode structure. For each channel, helium flow rate is 2.14 slm and oxygen flow rate is 10.7 sccm. For the single-channel structure (red), point *a* indicates its ignition point and point *b* indicates the voltage at which the single plasma jet reaches the downstream electrode.

array-housing unit and the ITO electrode were bridged in all seven channels by the plasma jets, the dissipated power was found to increase more quickly, as shown in figure 2(b). The jet plasmas became less capacitive and appeared more intense to the naked eye. At $V_p = 4.5$ kV, the total dissipated power is 600 mW or 85.7 mW per channel. This is equivalent to 3.1 W cm^{-3}, with an estimated plasma volume of 28 mm^3, and is about one order of magnitude larger than the typical dissipated power density of 0.3 W cm^{-3} in atmospheric helium dielectric barrier discharges sustained between two parallel plates at kHz frequencies [42]. The CAP jets are therefore potentially stronger plasmas, with higher plasma density than their counterparts between parallel electrodes.

The electrical characteristics of the 2D CAP jet array were in general similar to those of a comparable single jet, but they were quantitatively different. Figure 3 shows the increase of the dissipated power with increasing applied voltage for a single firing plasma channel and for the jet array case with all its seven plasma channels firing (marked in black). It is evident from figure 3 that the power–voltage relations are very similar in the two one-channel cases, regardless of whether the jet-housing structure is a single-channel device or a seven-channel array. An additional test was performed with all seven channels in the array structure connected to the power supply, but only the central channel supplied with He–O_2 gas, and this case was found to have a very similar voltage dependence of the dissipated power to that of other single-channel cases. In the absence of plasma jets, the equivalent capacitance of the array structure should be different from that of a single-channel device. The similarity of the one-channel cases suggests that electrical properties were dominated by the characteristics of the firing plasma jet, and that their difference from the jet-array case was mainly due to the difference in discharge properties.

At a given applied voltage, the jet array appeared to consume less electrical power per channel. For example, the one-channel cases consumed about 150 mW at $V_p = 4.5$ kV, where the array consumed 50% less at 75 mW per channel. This was probably a result of jet–jet interactions. It is also worth noting that plasma ignition in the one-channel cases occurred at approximately 0.8 kV (point '*a*' in figure 3) and the plasma jet reached the ITO electrode at $V_p = 3.3$ kV (point '*b*' in figure 3). For ease of reference, we refer to the latter as the bridging voltage at which plasma jets started to bridge the powered electrode to the downstream ground electrode. In the case of the jet array, the plasma ignition and bridging voltages were 1.1 and 2.3 kV, respectively. Therefore, compared to the case of one firing plasma channel, plasma ignition in the seven-channel array occurred at a higher applied voltage, but its jets reached the downstream ground electrode at a lower applied voltage. While the differences in the plasma ignition and bridging voltages can both be attributed to jet–jet interactions in general, the difference in the latter is understandable since the transport of neutral species and UV photons caused by one plasma jet should impact on the dynamics of its sounding jets. Less straightforward is, however, the difference in the voltage of plasma ignition, when the plasmas were just ignited and their interactions must have been very weak. Further insight into the jet–jet interaction mechanisms will be pursued in future investigations.

The above discussion mentioned that plasma ignition in the jet array started with the six surrounding channels. To see this clearly, and indeed to reveal the full course of plasma jet dynamics, we took nanosecond images at different points over one complete cycle of the applied voltage. In the first two columns in figure 4, five side views and their corresponding end views were captured in 10 ns exposure time during a negative half cycle of the applied voltage. It is evident that the central channel was ignited first, and it remained by far the strongest among the seven jets. However, no plasma jet ever reached the downstream ITO electrode. These are in a sharp contrast to the 10 ns images in the last two columns of figure 4 for a positive half cycle of the applied voltage. When the downstream ground electrode was the instantaneous cathode, plasma ignition started with the six surrounding channels and the ignition was simultaneous in all surrounding channels. Then ignition of the central channel followed. For the majority of the positive half cycle the central plasma jet had a weaker optical emission than the surrounding plasma jets. Therefore, in terms of the plasma emission intensity of the central channel and its six surrounding channels, the positive and negative half cycles were mirror images of one another. Another difference was that after ignition all seven jets reached the downstream ground electrode during the positive half cycle. In general, the optical emission intensity in the negative half cycle was much weaker than that in the positive half cycle (e.g. light intensities in figure 4 were normalized to their own maxima so that the two sets of side views are comparable and the two sets of end views are comparable). This explained the aforementioned observation that to the naked eye the six surrounding channels broke down first.

The temporal sequence of plasma ignition and its spatial dependence (i.e. the central channel versus the surrounding channels) have not been observed in 1D CAP jets [27], and are likely to be an important route to unlock the current puzzle of the jet–jet interaction mechanisms. The greater optical emission and the arrival of all seven jets at the downstream electrode in the positive half cycle are consistent with the common recognition that plasma jets are cathode-directed filaments or streamers. It is, however, useful to mention that we did not observe plasma bullets from the seven-jet array, although plasma bullets were routinely observed in a comparable single jet device [20, 43, 44].

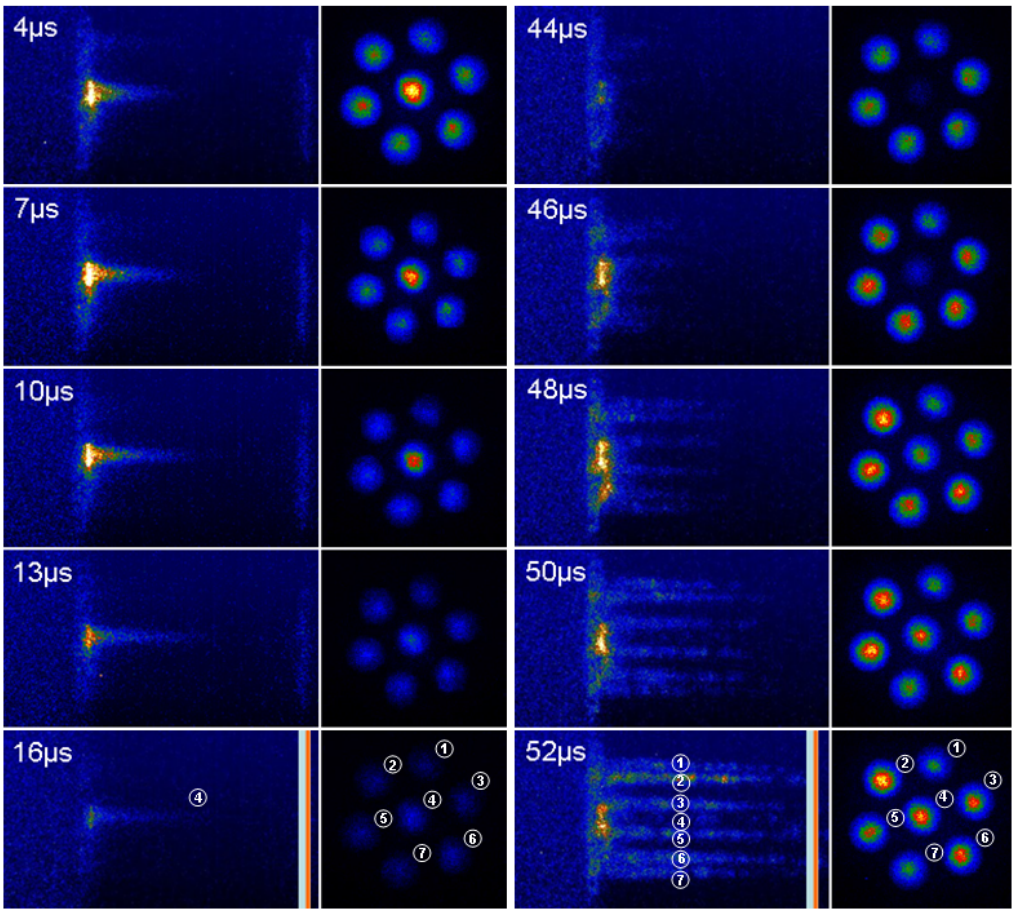

Figure 4. Side and end views of the seven-jet plasma array in 10 ns exposure time. The left two columns are for a negative half-cycle of the applied voltage, whereas the right two columns are for a positive half-cycle. Images in each column are normalized to their own maxima, so that the two sets of side views are comparable and the two sets of end view are comparable. The grey and orange vertical lines in the 16 μs image (in the first column) and the 52 μs image (in the third column) indicate the glass and the metal coating of the downstream ITO electrode.

4. Spatial distribution of jet reaction chemistry

The plasma dynamics of the seven jets in figure 4 exhibit a synchronized jet evolution, and a mirror contrast of jet emission intensities in the two different half cycles suggests the possibility that the optical emission of each plasma channel may average out over one complete cycle to become similar to one another. This suggests that on a timescale relevant to surface processing time (e.g. many seconds to a few minutes), the reaction chemistry delivered to a downstream surface by each plasma channel may have good channel–channel uniformity. We employed optical emission intensity as an indirect measure of reactive species and hence reaction chemistry, because of the difficulty of accessing reliable density measurements of the relevant reactive plasma agents, including electrons, oxygen atoms, nitric oxides and OH radicals.

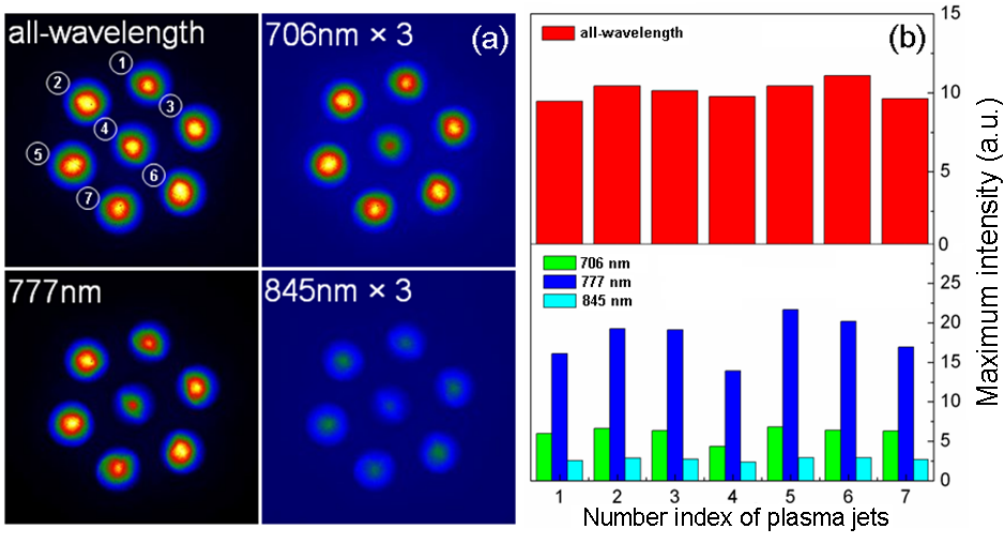

Figure 5. (a) Wavelength-integrated and wavelength-filtered end-view images, all taken in 100 μs exposure time, and (b) the jet–jet variation of the peak optical emission intensities at all wavelengths and at 706, 777 and 845 nm.

We considered wavelength-integrated optical emission as a broad indicator of plasma species as well as wavelength-filtered emission at 706, 777 and 845 nm. Helium line at 706 nm is known to represent energetic electrons [45], and recently it has also been linked to energetic electrons in RF atmospheric microplasmas [46]. Excited atomic oxygen lines at 777 and 845 nm are relevant because of their direct relation to ground-state oxygen atoms, which have been implicated in both microbial inactivation [4], [7]–[10], [47] and protein reduction [48]–[50]. Without being limited to specific applications, energetic electrons and oxygen atoms are representative of important plasma agents for plasma medicine.

Figure 5(a) shows end views of the optical emission patterns of the seven-jet array with an exposure time of 100 μs (i.e. one period of the applied voltage), both wavelength integrated and filtered for 706, 777 and 845 nm. The peak applied voltage was 2.6 kV. Emission intensities at 706 and 845 nm were comparatively weak compared to that at 777 nm and that obtained from wavelength integration, and were multiplied by a factor of 3 to bring the emission intensities of all four cases to a similar level. The four cases in figure 5 are very similar and indicate good uniformity of reactive species and electrons delivered by individual plasma jets. Figure 5(b) provides a more direct indication of the jet–jet uniformity, particularly in the case of full wavelength (i.e. wavelength integrated) and 845 nm. Their jet–jet variation of emission intensity was found to be 5.6% and 7.9%, respectively. On the other hand, the jet–jet variation at 706 and 777 nm was larger at 13.5% and 14.7%, respectively. In our experiments, the plasma–substrate interaction was subject to environmental interference without any control chamber and no individual ballast was used. Therefore, the variations could be reduced further. The applied voltage was slightly above the value of the bridging voltage and therefore the plasma jets were not very strong and likely to be susceptible to environmental interference. Given these, the jet–jet variations in the four cases of figure 5 were encouragingly small.

It is of interest to see whether the above uniformity of downstream reactive species could be maintained over a shorter timescale. If so, it suggests a persistent uniformity underpinned

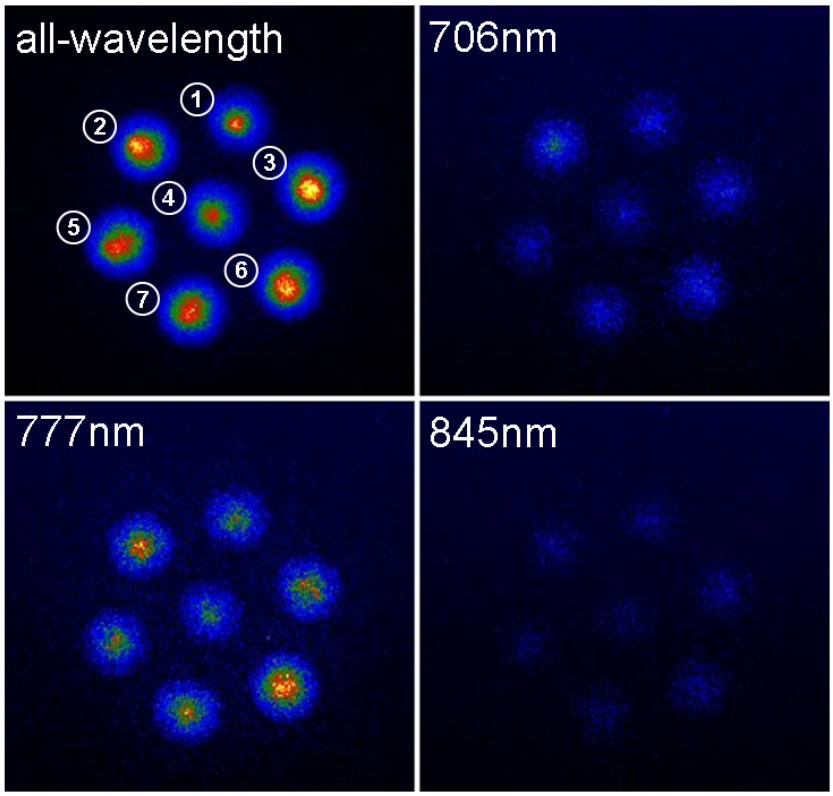

Figure 6. End-view images of the same four cases again at a peak applied voltage of 2.6 kV but with 10 ns exposure time.

by the in-built control of jet–jet interaction and plasma–surface interaction. Figure 6 shows end-view images of the same four cases again at a peak applied voltage of 2.6 kV but with 10 ns second exposure time. Good uniformity is evident. Detailed evaluation found that on a 10 ns timescale the jet–jet variation of all wavelength emission intensity was 11.9%, whereas that of wavelength-filtered emission was 6.5%, 8.5% and 3.3% at 706, 777 and 845 nm, respectively. Overall these numbers were slightly lower than those for over 100 μs. It should be noted from figure 4 that jet–jet variations on a 10 ns scale tended to change depending on when the image was taken. Therefore the variation percentage on the 10 ns scale in figure 6 may not be representative. However, they were similar to those over 100 μs, suggesting a persistent uniformity. Therefore, the array structure of figure 1 appears to have an in-built control mechanism, probably by means of feedback, with which the jet–jet interactions were well controlled (thus all jets firing simultaneously), and the plasma–substrate interactions were also well controlled (hence good uniformity in jet-delivered reaction chemistry). In two separate but related studies, we discovered that the radial impact of jet-delivered downstream reaction chemistry goes beyond the physical confines of the plasma jet diameter [36, 50]. In other words, the surface areas between any two adjacent plasma contact points in the substrate surface are also under the influence of jet-delivered reaction chemistry. This implies that CAP jet arrays such as that in figure 1 could be used for large surface treatment with minimum movement.

The spatial uniformity of plasma-jet-delivered reaction chemistry shown in figures 4–6 was established with an oxygen admixture of 0.5%. To evaluate whether this remains true at

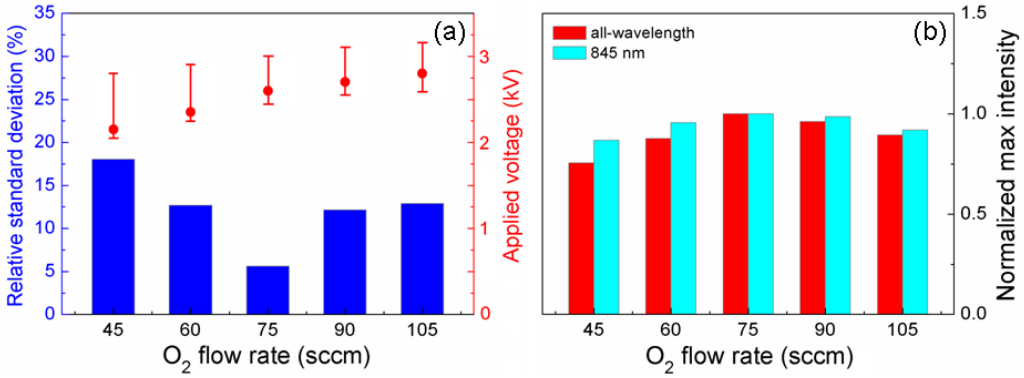

Figure 7. Jet–jet uniformity measured in (a) RSD and (b) normalized maximum emission intensity, both wavelength integrated and filtered at 845 nm.

other O_2/He ratios, fast imaging experiments were repeated for O_2/He = 0.3–0.7%. As shown in figure 7(a), the lowest relative standard deviation (RSD) of 5% is reached at an oxygen flow rate of 75 sccm or O_2/He = 0.5%. When the O_2/He ratio changes by 0.1% to either 0.4 or 0.6%, RSD increases significantly to 12% from 5%. As the oxygen admixture changes, the applied voltage at which the best jet–jet uniformity is achieved also changes, and the range of its change is about 0.9–1.1 kV (shown in figure 7(a)). Under the conditions for the best jet–jet uniformity for O_2/He = 0.3–0.7%, it was found that the highest optical emission also occurred at O_2/He = 0.5%. This is of course desirable for practical applications, and is shown in figure 7(b), where both wavelength-integrated intensity and intensity at 845 nm are normalized to their respective values for O_2/He = 0.5%. The maximum oxygen admixture for all seven jets to form was found to be 0.8% under our experimental conditions.

5. Conclusions

As an alternative to current large-scale CAP sources used in plasma medicine, a generic class of 2D CAP jet arrays have been studied. These are SEAPA, particularly suited for delivering reaction chemistry to uneven objects, and complementary to spatially confined atmospheric plasma arrays (SCAPA), predominately used for photonics [33, 34]. An in-built ballasting feature of the array structure and well engineered power electronics have been used to control effectively the jet–jet interactions and the plasma–sample interactions. Fast imaging with wavelength-filtered 2D optical emission maps has demonstrated excellent uniformity in reaction chemistry delivered by individual jets to the downstream sample surface. This spatial uniformity has been shown to possess a rich group of dynamic features, for example the central jet of the honeycomb-arranged array is the strongest in the negative half cycle, whereas the six surrounding jets are the strongest (equally) in the positive half cycle. These dynamic features offer possible insights with which to better control the jet–jet interactions and the plasma–surface interactions in future studies. Finally, it has been found that the best uniformity and the highest optical emission are both achieved at an oxygen admixture of 0.5% into the background helium flow.

References

[1] Fridman G, Friedman G, Gutsol A, Shekhter A B, Vasilets V N and Fridman A 2008 *Plasma Process Polym.* **5** 503
[2] Laroussi M 2009 *IEEE Trans. Plasma Sci.* **37** 714
[3] Morfill G E 2009 The Munich plasma medicine project: results and current status *2nd Int. Conf. Plasma Medicine* (*San Antonio, TX, USA, 16–20 March*)
[4] Deng X T, Shi J and Kong M G 2006 *IEEE Trans. Plasma Sci.* **34** 1310
[5] Iza F, Kim G J, Lee S M, Lee J K, Walsh J L, Zhang Y T and Kong M G 2008 *Plasma Process. Polym.* **5** 322
[6] Stoffels E, Sakiyama Y and Graves D B 2008 *IEEE Trans. Plasma Sci.* **36** 1441
[7] Deng X T, Shi J, Shama G and Kong M G 2005 *Appl. Phys. Lett.* **87** 153901
[8] Sato T, Miyahara T, Doi A and Ochiai S 2006 *Appl. Phys. Lett.* **89** 073902
[9] Yu H, Perni S, Shi J J, Wang D Z, Kong M G and Shama G 2006 *J. Appl. Microbiol.* **101** 1323
[10] Laroussi M, Tendero C, Lu X, Alla S and Haynes W L 2006 *Plasma Process. Polym.* **3** 470
[11] Deng S, Ruan R, Mok C K, Huang G, Lin X and Chen P 2007 *J. Food Sci.* **72** M62
[12] Perni S, Liu D W, Shama G and Kong M G 2008 *J. Food Protect.* **71** 302
[13] Perni S, Shama G and Kong M G 2008 *J. Food Protect.* **71** 1619
[14] Selcuk M, Oksuz L and Basaran P 2008 *Bioresour. Technol.* **99** 5104
[15] Stoffels E, Flikweert A J, Stoffels W W and Kroesen G M W 2002 *Plasma Sources Sci. Technol.* **11** 383
[16] Fridman G, Shereshevsky A, Jost M M, Brooks A D, Fridman A, Gutsol A, Vasilets V and Friedman G 2007 *Plasma Chem. Plasma Process.* **27** 163
[17] Kim G C, Kim G J, Park S R, Jeon S M, Seo S J, Iza F and Lee J K 2009 *J. Phys. D: Appl. Phys.* **42** 032005
[18] Lee H J, Shon C H, Kim Y S, Kim S, Kim G C and Kong M G 2009 *New J. Phys.* **11** 115026
[19] Schutze A, Jeong J Y, Babayan S E, Park J, Selwyn G S and Hicks R F 1998 *IEEE Trans. Plasma Sci.* **26** 1685
[20] Teschke M, Kedzierski J, Finantu-Dinu E G, Korzec D and Engemann J 2005 *IEEE Trans. Plasma Sci.* **33** 310
[21] Walsh J L and Kong M G 2007 *Appl. Phys. Lett.* **91** 221502
[22] Laroussi M and Akan T 2007 *Plasma Process. Polym.* **4** 777
[23] Leveille V and Coulombe S 2005 *Plasma Sources Sci. Technol.* **14** 467
[24] Lu X P, Cao Y G, Yang P, Xiong Q, Xiong Z L, Xian Y B and Pan Y 2009 *IEEE Trans. Plasma Sci.* **37** 668
[25] Lee H W, Kim G J, Kim J M, Park J K, Lee J K and Kim G C 2009 *J. Endod.* **35** 587
[26] Jiang C, Chen M T, Schaudinn C, Gorur A, Vernier P T, Costerton J W, Jaramillo D E, Sedghizadeh P P and Gundersen M A 2009 *IEEE Trans. Plasma Sci.* **37** 1190
[27] Cao Z, Walsh J L and Kong M G 2009 *Appl. Phys. Lett.* **94** 021501
[28] Yang X, Moravej M, Nowling G R, Chang J P and Hicks R F 2005 *IEEE Trans. Plasma Sci.* **33** 294
[29] Shimizu K, Sugiyama T and Samaratunge M N L 2008 *IEEE Trans. Ind. Appl.* **44** 506
[30] Shenton M J and Sevens G C 2001 *J. Phys. D: Appl. Phys.* **34** 2761
[31] Czylkowski D, Jasinski M, Mizeraczyk J and Zakrzewski Z 2006 *Czech. J. Phys.* **56** B684
[32] Shimizu T, Steffes B, Pompl R, Jamitzky F, Bunk W, Ramrath K, Georgi M, Stolz W, Schmidt H U, Urayama T, Fujii S and Morfill G E 2008 *Plasma Process. Polym.* **5** 577
[33] Eden J G and Park S J 2006 *Phys. Plasmas* **13** 057101
[34] Sakai O, Sakaguchi T and Tachibana K 2007 *J. Appl. Phys.* **101** 073304
[35] Walsh J L, Shi J J and Kong M G 2006 *Appl. Phys. Lett.* **88** 171501
[36] Cao Z, Nie Q, Walsh J L, Ren C S, Wang D Z and Kong M G 2009 *Plasma Sources Sci. Technol*. submitted
[37] Koretzky E and Kuo S P 1998 *Phys. Plasmas* **5** 3774
[38] Kuo S P, Koretzky E and Orlick L 1999 *IEEE Trans. Plasma Sci.* **27** 752
[39] Hubicka Z, Cada M, Sicha M, Churpita A, Pokorny P, Soukup L and Jastrabık L 2002 *Plasma Sources Sci. Technol.* **11** 195

[40] Foest R, Kindel E, Ohl A, Stieber M and Weltmann K D 2005 *Plasma Phys. Control. Fusion* **47** B525
[41] Walsh J L and Kong M G 2008 *Appl. Phys. Lett.* **93** 111501
[42] Kong M G and Deng X T 2003 *IEEE Trans. Plasma Sci.* **31** 7
[43] Lu X and Laroussi M 2006 *J. Appl. Phys.* **100** 063302
[44] Shi J, Zhong F, Zhang J, Liu D W and Kong M G 2008 *Phys. Plasmas* **15** 013504
[45] Nersisyan G and Graham W G 2004 *Plasma Sources Sci. Technol.* **13** 582
[46] Liu D, Iza F and Kong M G 2009 *Appl. Phys. Lett.* **95** 031501
[47] Perni S, Shama G, Hobman J L, Lund P A, Kershaw C J, Hidalgo-Arroyo G A, Penn C W, Deng X T, Walsh J L and Kong M G 2007 *Appl. Phys. Lett.* **90** 073902
[48] Deng X T, Shi J J, Chen H L and Kong M G 2007 *Appl. Phys. Lett.* **90** 013903
[49] Deng X T, Shi J J and Kong M G 2007 *J. Appl. Phys.* **101** 074701
[50] Bayliss D B, Walsh J L, Shama G, Iza F and Kong M G 2009 *New J. Phys.* **11** 115024